



Multivariate forest structure modelling and mapping using high resolution airborne imagery and topographic information

Jon Pasher*, Douglas J. King

Department of Geography and Environmental Studies, Geomatics and Landscape Ecology Laboratory, Carleton University, 1125 Colonel By Drive, Ottawa, Ontario, Canada K1S 5B6

ARTICLE INFO

Article history:

Received 12 December 2008
Received in revised form 3 February 2010
Accepted 6 March 2010

Keywords:

High spatial resolution remote sensing
Forest structure
Image spatial analysis
Redundancy Analysis (RDA)
Predictive modelling
Multivariate analysis

ABSTRACT

Remote sensing has been widely used for modelling and mapping individual forest structural attributes, such as LAI and stem density, however the development and evaluation of methods for simultaneously modelling and mapping multivariate aspects of forest structure are comparatively limited. Multivariate representation of forest structure can be used as a means to infer other environmental attributes such as biodiversity and habitat, which have often been shown to be enhanced in more structurally diverse or complex forests. Image-based modelling of multivariate forest structure is useful in developing an understanding of the associations between different aspects of vertical and horizontal structure and image characteristics. Models can also be applied spatially to all image pixels to produce maps of multivariate forest structure as an alternative to sample-based field assessment. This research used high spatial resolution multispectral airborne imagery to provide spectral, spatial, and object-based information in the development of a model of multivariate forest structure as represented by twenty-four field variables measured in plots within a temperate hardwood forest in southern Quebec, Canada. Redundancy Analysis (RDA) was used to develop a model that explained a statistically significant proportion of the variance of these structural attributes. The resulting model included image variables representing mostly within-crown and within-shadow brightness variance (texture) as well as elevation, taken from a DEM of the study area. It was applied spatially across the entire study area to produce a continuous map of predicted multivariate forest structure. Bootstrapping validation of the model provided an RMSE of 19.9%, while independent field validation of mapped areas of complex and simple structure showed accuracies of 89% and 69%, respectively. Multiscale testing using resampled imagery suggested that the methods could possibly be used with current pan-sharpened, or future sub-metre resolution, multispectral satellite imagery, which would provide much greater spatial coverage and reduced image processing compared to airborne imagery.

© 2010 Elsevier Inc. All rights reserved.

1. Introduction

Monitoring forest structure is an important application of remote sensing, with many individual structural attributes, as well as multivariate aspects, modelled and mapped at a variety of scales. Forest structural information derived from remotely-sensed imagery can be used for enhancing forest inventories (e.g. Lefsky et al., 2001; Wulder, 1998), assessing and mapping disturbance and damage (e.g. Cosmopoulos and King, 2004; Olthof et al., 2004; Wulder et al., 2008), as well as deriving potential indicators of forest habitat/biodiversity (e.g. Coops and Catling, 1997a,b; Pasher and King, 2009; Pasher, 2009).

Commonly mapped individual structural attributes, including Leaf Area Index (LAI), canopy closure, basal area, tree height and various attributes of dead trees, have been examined using a variety of sensors, including airborne synthetic aperture radar (SAR) (e.g. Breidenbach

et al., 2008; Nelson et al., 2007), lidar (e.g. Breidenbach et al., 2008; Lefsky et al., 2002; Lim et al., 2003), optical satellite data (e.g. Fernandes et al., 2003; Hall et al., 2006), and optical airborne data (e.g. Franklin et al., 2000; Hall et al., 2003), which is the focus of the research presented here. Airborne optical data has some clear advantages over radar and lidar, including the generally lower acquisition and processing costs for small coverages, greater availability in terms of the number of airborne digital cameras in commercial operation, and finally, more straightforward interpretation based on a long tradition of photographic image analysis.

Two general approaches to forest structure modelling using remotely-sensed data include radiative-transfer and empirical modelling, the former relying mainly on spectral information (e.g. Leblanc and Chen, 1998; Peddle et al., 2004) with limited modelling having been carried out using spatial information (e.g. Bruniquel-Pinel and Gastellu-Etchegorry, 1998; Gastellu-Etchegorry et al., 1996). On the other hand, while empirical studies have commonly incorporated image spectral information, perhaps more importantly they have often used image spatial information in various forms, including image texture (e.g. Olthof

* Corresponding author. Tel.: +1 613 520 2600x8439; fax: +1 613 520 4301.
E-mail address: jpasher@rogers.com (J. Pasher).

and King, 1997; Wulder et al., 1998), spatial dependence measures such as semivariance (e.g. Johansen and Phinn, 2006; Lévesque and King, 1999; Treitz and Howarth, 2000), radiometric fractions at the pixel level (e.g. Pellikka et al., 2000; Seed and King, 2003) or at the subpixel level using spectral unmixing (e.g. Lévesque and King, 2003; Pasher et al., 2007; Peddle et al., 1999) or combinations of these (e.g. Lévesque and King, 2003).

Modelling multivariate aspects of forest structure using remote sensing, in terms of the interaction of multiple attributes, as opposed to individual structural attributes, is comparatively limited in the literature (Coops and Catling, 1997a,b; Coops et al., 1998; Sampson et al., 2001; Cosmopoulos and King, 2004; de la Cueva, 2008; Lefsky et al., 2005; Wunderle et al., 2007). This is particularly true for research pertaining to hardwood forests with Sampson et al. (2001) being the only example found. Previous studies can be organized into two methodological groups: 1) those that first define a multivariate field-based index of forest structure independent of remotely-sensed data and then typically regress it against multiple image variables to determine how well the image variables can predict the given structural index, and 2) those that explore and determine the types of relationships between image information and forest structural attributes, using the resulting relationships as a means to model and map multivariate forest structure. Each is summarized below for some example studies.

As an example of the first methodological group, Coops and Catling (1997a,b), followed by Coops et al. (1998), modelled a pre-defined subjective visually-based field complexity score using 2 m resolution visible and near-infrared (NIR) digital airborne videography. Local NIR band variance extracted over the canopy or from within automatically segmented crowns was found to be strongly correlated with the complexity score, illustrating that more complex forest structures were manifested in increased crown and canopy spectral heterogeneity. In another approach Wunderle et al. (2007) used Principal Components Analysis (PCA) of field measured data to create what was termed a 'structural complexity index' for regenerating conifer stands that represented 79% of the variance in the structural attributes. They then produced a regression model (adjusted $R^2 = 0.74$, $p < 0.001$) of the index against three spectral and spatial image variables extracted from pan-sharpened SPOT imagery that was then validated using a withhold-one jackknife approach. The model generally overestimated the actual index value, a result that was attributed to the fact that stands less than five years old (i.e. recently cut) had several parameters equal to zero (e.g. crown closure, stem density, and average dbh).

One of the most thorough examinations of field-based structural indices was presented by McElhinny et al. (2006), who also developed a robust, objective, and quantitative methodology for combining a set of field-based measures of forest structure into a single value representing overall forest structure. Their method involved scaling the individual measures to a score from 0 to 10 using a regression analysis that fit the raw values to quartile midpoints calculated from the variable's distribution across the study sites. The rescaled values were then combined into a simple additive index. These field-based scores or indices can be used to summarize plot-based forest structure, which although not conducted in their study, could potentially be modelled using remotely sensed variables.

In the second methodological group, multivariate statistical techniques are commonly used to determine a model relating a set of image metrics to a set of field measured forest attributes. This differs from the first group where field variables are first combined irrespective of how well they are related to, or manifested in remotely sensed imagery. Some studies have used Canonical Correlation Analysis (CCA) of a set of image variables against a set of field variables to evaluate the type and strength of relationships. The derived field-variable canonical variates are then commonly regressed against the image variables to produce a predictive model. In this method, and in regression of image data against a pre-defined index as described above, PCA is often first applied independently to the image and field data to produce orthogonal

variables and reduce dimensionality. Other studies in the second group have used Redundancy Analysis (RDA) to derive a predictive multivariate model directly without the need to interpret derived principal components or canonical variates. This is the approach that was taken for this research.

An example of the second group that used CCA is Jakubauskas (1996), where linear relations between forest structural variables and Landsat derived image variables were examined. Based on that work, Olthof and King (2000) used CCA to model forest structure using 50 cm pixel airborne digital camera image variables in a mixed boreal forest. The first canonical component defined a significant multivariate relationship between structure and image variables and was termed a forest structure index (FSI). Cosmopoulos and King (2004) refined the FSI and assessed the potential to apply it in a temporal analysis of structural change. To reduce dimensionality, the CCA was implemented using the first three principal components of the nine field variables representing 81.3% of their original variance, and the first four principal components of the twelve spectral, texture and image fraction variables, accounting for 80% of their original variance. This process reduced some of the variance accounted for in the model and also required interpretation of the meaning of each of the principal components in order to understand the meaning of the resulting FSI.

An example of the second group that used RDA is Sampson et al. (2001) who modelled structural variables against spectral indices derived from CASI (Compact Airborne Spectrographic Imager) imagery in three silviculturally treated portions of a hardwood forest near Sault Ste. Marie, Ontario, Canada. Their results showed significant, but admittedly weak, relations, which were held together by the inclusion of the clearcut plots in the analysis, with canopy openness accounting for most of the variance in the field data. de la Cueva (2008) used RDA to model structural variables against fourteen Landsat 7 ETM+ spectral indices and topographic variables in order to differentiate between three forest types in western Spain, which were individually dominated by conifers, evergreen sclerophyll, and deciduous trees. RDA was carried out separately for each type of vegetation. The results reported the best five explanatory image variables for each RDA model using a forward selection method. They showed a maximum explanation of the field variance of 24% (ranging from 6 to 24%) using a combination of the first and second RDA axes, which was lower than the author had expected.

1.1. Research objectives

The objectives of the research presented in this paper were:

1. Develop a geomatics-based method using high spatial resolution multispectral airborne remote sensing and topographic information for modelling multivariate structure within a temperate hardwood forest. The particular use of RDA that is presented with high resolution imagery, and including such a variety of spectral, spatial, object and topographic variables, many which have not been previously incorporated into such modelling in a hardwood forest, is a unique aspect of this research.
2. Map predicted multivariate forest structure continuously across the study area using an empirical model derived through RDA, including independent map validation using field information.
3. Explore the potential for modelling and mapping multivariate forest structure at multiple scales using simulated lower spatial resolution imagery.

This research is part of a larger project on the development of remote sensing-based structural indicators of habitat and biodiversity within a temperate hardwood forest. While the portion of the research presented in this manuscript focuses on modelling and mapping from a remote sensing perspective, a companion paper has been submitted that presents extensive details of the modelling aspects of the research from an ecological perspective in terms of the field measurements of forest structure and the potential use of a

multivariate forest structure model derived from image data as an ecological indicator for habitat and biodiversity (also available in Pasher (2009)).

2. Methods

2.1. Study area

The research was carried out in Gatineau Park, which extends from about 20–50 km NW of the city of Ottawa, Canada. More than 80% of the Park's approximately 36,000 ha are forested, with the overstorey in the study area dominated by sugar maple (*Acer saccharum* Marsh.). Smaller numbers of species such as American beech (*Fagus grandifolia* Ehrh.), red oak (*Quercus rubra* L.), red maple (*Acer rubrum* L.), American basswood (*Tilia americana* L.), ironwood (*Ostrya virginiana* (Mill.) K. Koch), and white birch (*Betula papyrifera* Marsh.), amongst other species are also present. The composition of this mature temperate hardwood forest is partially a result of the historical logging of white pine (*Pinus strobus*) during the late nineteenth and early twentieth centuries. The forest also experienced patchy damage from a major ice storm in January 1998, which provided a wide range of structural conditions suitable for gradient-based modelling. The Park's topography consists of rolling hills with elevation variations of up to approximately 300 m (King et al., 2005; Lopoukhine, 1974; NCC, 2005).

The study area was selected for continuity following successful ice storm damage modelling and mapping research (King et al., 2005). It was approximately 4.5 km north-south and 400 m wide (~180 ha) (Fig. 1), and was aligned with one of the sampling transects from previous studies (King et al., 2005; Pellikka et al., 2000). The use of an elongated area minimized the number of flightlines needed for image acquisition as a result of the small sensor view angle (see below).

2.2. Field measurement of forest structure

In the summer of 2007, fifty field sites were selected across the study area to be representative of the range of structural conditions and topographic settings. As described in detail in Pasher (2009), the plots were located to provide a representative range (assessed qualitatively) of overstorey tree sizes and positions, canopy closure, understorey and ground vegetation amounts, and the amount of standing and fallen dead wood. At each site a 20 m × 20 m field plot was established. This plot size was selected based on previous image lacunarity analysis in the same forest to determine the optimal spatial extent for image feature extraction (Butson and King, 2006) that showed pattern scales of up

to 14 m. Semivariogram range of field measured crown diameter was also about 14 m (Butson and King, 1999). Thus, to be conservative and to provide enough sample trees in sparser plots, in subsequent studies in the Park a plot size of 20 m × 20 m has been used. The coordinates of the plots were collected using a differential GPS with an external antenna and WAAS enabled, with post-processing using the Gatineau SOPAC base station (CAGS), located approximately 10 km from the study area. Using these techniques, horizontal accuracy was expected to be better than 1 m.

Structural attributes measured in each plot were selected following a literature survey of common measures used to represent forest structure and multivariate structural indices (e.g. McElhinny et al., 2005; Neumann and Starlinger, 2001; Spies and Franklin, 1991) and based on their expected manifestation in the imagery (see Section 2.4). In general, they represented structure either directly (e.g. crown size, canopy closure) or indirectly (e.g. large coarse woody debris associated with overstorey gaps). As commonly applied in other studies, more complex vertical structure was typified by an abundance of ground and understorey vegetation and was observed to occur where there was significant overhead canopy openness. Note that in the study plots the maximum openness was about 50%. As this paper focuses on the remote sensing aspects of the study, only a summary of the field measured attributes is provided (Table 1). A detailed description of the structural attributes, why they were chosen, and how they were measured or derived is provided in Pasher (2009). Of the fifty field ten had relatively simple forest structure and eleven had relatively complex structure. Based on an initial qualitative assessment, the remaining twenty-nine plots represented what was considered to be typical structural conditions in this area of the hardwood forest.

2.3. Airborne imagery acquisition and processing

On August 21st, 2007, three-band (green 500–600 nm, red 600–700 nm, and near infrared 750–850 nm) imagery was acquired using a DuncanTech MS4100 1940 × 1020 digital CIR camera with a Nikon 24 mm lens mounted vertically in a modified door attached to a Cessna-172 aircraft. The flight altitude was 650 m in order to achieve 20 cm nominal ground pixel size, which was selected based on previous forest structure research in the park as well as the desire to detect and delineate individual forest objects, including tree crowns, crown clusters and dead branches. Imagery was acquired from South to North along two flightlines (Fig. 2), resulting in eighty-eight images with ~30% forward and side overlap.

Each image was cropped to 1080 pixels × 1080 pixels (~216 m × 216 m ground coverage), representing a maximum view angle of 9.5° in both the x and y directions. This angle was selected based on previous research (Seed and King, 2003), that showed significant negative effects of view angles beyond 10° on forest structure modelling. The imagery was acquired under sunny conditions between 1:37 and 1:48 pm, just after solar noon, with solar zenith and azimuth angles of 33.7° and 190.2°, respectively. The sensor system allowed image histograms to be viewed in-flight so exposure times were manually optimized for each band over adjacent forested areas before acquiring the data.

Typically, airborne imagery has brightness variations caused by sun-sensor-surface geometry. Specifically, image brightness is effected by bi-directional reflectance variation (BRV), topographic variations as well as lens effects (light fall-off and optical vignetting). BRV effects were reduced in image acquisition by limiting the view angle (i.e. 9.5°) and the spatial non-uniformity of the camera lens response was reduced through pre-flight calibration (Geospatial Systems Inc., 2007). Despite these adjustments, profiles across the images showed that average forest brightness in flat terrain increased from the bottom to the top of the imagery (in the direction of flight and plane of the sun) by approximately 2–6% in the green and NIR bands, and up to 35% in the red band. Additionally, topographic brightness variations were evident between north and south facing slopes, which were the dominant aspects in this area. Sampled crowns

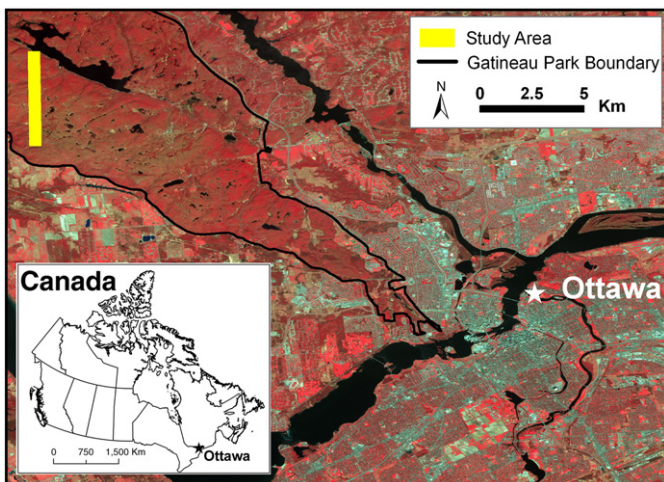


Fig. 1. Location of study area within the southern section of Gatineau Park near Ottawa, Canada. Shown with 2005 SPOT satellite image in the background (courtesy P. Pellikka, University of Helsinki).

Table 1

Summary of measured attributes representing the various aspects of forest structure. A full description is given in Pasher and King (submitted).

Structural attributes	Measurements and sampling methods	Derived variables
Overstorey trees (>10 cm dbh)	dbh (cm); height (m); crown diameter (m)	# of trees; # of large trees (>35 cm dbh); \bar{x} and S.D. for each plot; live basal area (m ² /ha)
Tree spacing	Nearest neighbour (NN) distance (m) between overstorey trees	\bar{x} for each plot
Canopy openness and LAI	Hemispherical photographs (camera height: 1 m and 6 m)	Openness (0°–60°) (%) and LAI (55°–60°) derived for each height; change between heights
Ground and understorey vegetation	5 height classes, along diagonals every 50 cm: <10 cm, 11–50 cm, 51 cm–1 m, 1–2 m, and >2 m	% of plot covered by vegetation in each class
Snags	Presence; dbh (cm); height (m)	# of snags; \bar{x} and S.D. for each plot; dead basal area (m ² /ha)
Coarse woody debris (>7.5 cm diameter)	Sampled along plot diagonals	# of pieces

\bar{x} = average calculated for all trees or snags in the plot.

S.D. = standard deviation calculated for all trees or snags in the plot.

extracted from opposite sides of a valley showed that the south facing slope had brightness averages 6–22% higher than north facing slopes in the three spectral bands. In order to compare different areas of the imagery to each other and to develop multivariate models of forest structure from image brightness and spatial information, these residual brightness variations were removed.

A variety of methods have been widely used to correct for BRV in imagery (including empirical methods (Pellikka, 1998; Pickup et al., 1995) and theoretical BRDF modelling methods (Li and Strahler, 1992; Omari et al., 2009). Common topographic corrections include the cosine correction, c-correction, Minnaert Correction, and statistical-empirical corrections (e.g., Teillet et al., 1982; Meyer et al., 1993; Soenen et al., 2005). However, in tests using 2005 imagery collected with the same camera over the same forest of this research, Bemrose (2006) found that many of these methods overcorrected the imagery causing flare-ups towards the edges and that an empirical net brightness correction can

be more effective in reducing overall brightness variations across an image scene of uniform land cover such as the forest. A net image correction can also be applied in one step, eliminating the need for separate BRV, sensor, optical, and topographic correction algorithms. Tests of net correction methods presented in Richter (2005) and Cosmopoulos and King (2004), as well the c-correction method, showed inconsistent results and overcorrection in many areas, so a simple net correction was implemented as described below.

Non-forest was manually masked out of each image and the general brightness trend across each band was calculated using a large moving window average filter (99×99 pixels). The output images were normalized from 0 to 1 and inverted to create a correction template for each band that was multiplied by each acquired airborne image (Fig. 3). An algorithm based on Nielsen (2004) was then used to match each image histogram to that generated for a set of master images acquired over flat terrain.

In the output images, crowns and shadows were examined at different locations comparing nadir and off nadir pixels in flat and sloped areas. For all three spectral bands, there were no significant differences ($p < 0.001$) in DN values found for these image samples. As well, while the correction procedure left the images looking spectrally “flat”, this was simply a result of the view scale (e.g. Fig. 3). Figs. 4 and 6 show the retained image detail at full resolution. It should also be noted that this correction procedure reduced or removed topographic brightness variations as desired, but as structural variations were expected to be related to topography, topographic data were used directly for modelling as described later.

Following this correction procedure, the eighty-eight images were mosaicked together (positional RMSE < 5 pixels (~1 m)). In the overlap region between each image pair, the image data representing radiance backscatter were retained in the mosaic (based on test results from Seed and King (2003)). The mosaic was manually georeferenced to two 2004, 25 cm leaf-off orthophotos (NCC, 2004) using a thin plate exact fit spline with thirty-eight control points. The resulting RMSE for twenty-nine independent test points was 2.56 m (X) and 2.29 m (Y). This georeferencing error, combined with that of the mosaic procedure (~1 m error) and the field plot GPS position error (~1 m), resulted in a combined RMSE of ~3 m in both the X and Y directions, or approximately 15% of the plot size. This error was considered to be small enough to not affect extraction of image information from the plots as none were located close to significant changes in forest structure or land cover.

2.4. Image variable selection and extraction from airborne imagery

A suite of variables was extracted from the imagery based on results from other studies of empirical modelling of forest structural attributes as well as based on their expected response to the varied structure in the forest. They represented: 1) spectral information, including radiometric fractions at the pixel and subpixel level, 2) spatial information calculated from the gray-level co-occurrence

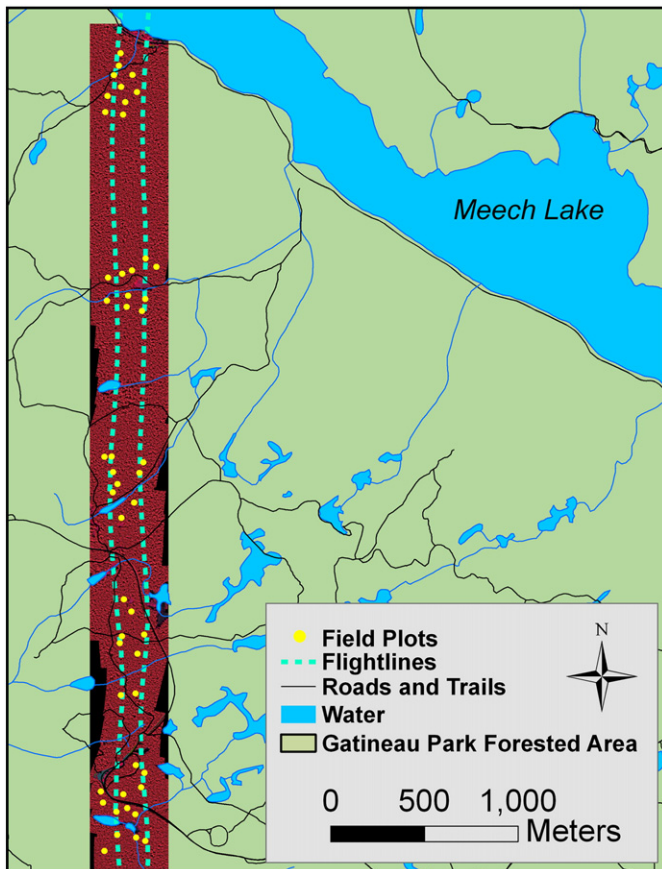


Fig. 2. The final multispectral image mosaic showing the two flightlines and the fifty field plots.

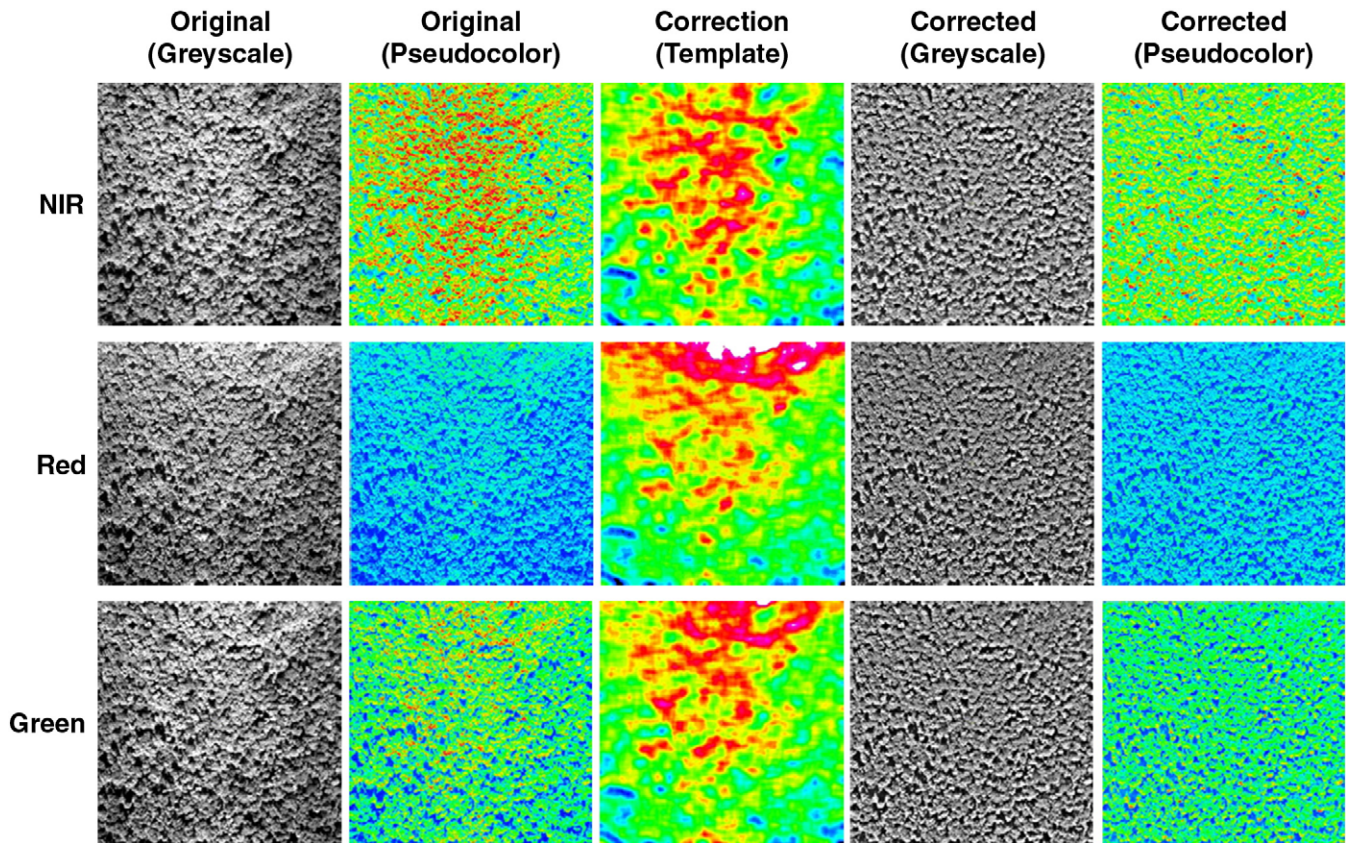


Fig. 3. Net image correction process and results shown for a sample image, with each individual original spectral band shown, along with corresponding correction templates, and the corresponding corrected images.

matrix (GLCM) and semivariograms, and 3) canopy and shadow object-based information. Details of each are given in the following paragraphs. The suite of variables selected represented the major within-crown, within-shadow, and canopy level spectral and spatial properties contained in the imagery. Data for all variables (within-

crown, within-shadow, canopy level) were generated for each plot. The mean and standard deviation over the plot were calculated except for variables where only a single value was generated for the whole plot.

2.4.1. Image spectral variables

The plot average image brightness of each spectral band, as well as NDVI was extracted with the expectation of lower image brightness in more structurally complex canopies with a greater mix of crowns and shadows than in more uniform closed canopies. Similar to Seed and King (2003), unsupervised ISODATA clustering was used to classify the imagery into thirty clusters that were then aggregated to create a map of forest canopy, shadow, and exposed wood. The percentage of each plot covered by these three classes and their average brightness in each spectral band were extracted. Additionally, constrained linear spectral unmixing was used, with endmembers manually extracted from the imagery, in order to extract subpixel fractions and average plot brightness of sunlit canopy, shadow, and exposed wood (Lévesque and King, 2003; Pasher et al., 2007; Peddle et al., 1999).

2.4.2. Image spatial variables

Areas of more complex forest structure were expected to be associated with greater spatial variability in image brightness due to the greater presence of gap shadows and mutual shading due to varied overstorey tree crown heights. As a first order texture measure, the standard deviation of plot image brightness was extracted for each spectral band. Second order texture measures were extracted from the first component calculated from a PCA of the three spectral bands (94.9% of total variance). Five commonly used GLCM texture measures (Contrast, Entropy, ASM, Correlation, and Homogeneity) (Haralick et al., 1973), which have been shown to be useful for modelling forest structure attributes (Cosmopoulos and King, 2004; Franklin et al., 2000;

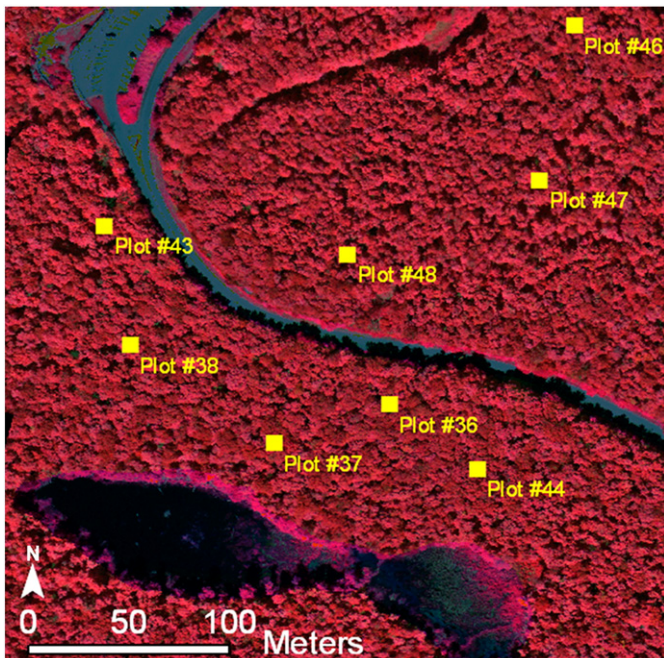


Fig. 4. Subset of multispectral image mosaic, spanning across the seams of multiple images, following brightness corrections. Locations of some of the field plots are shown.

Kayitakire et al., 2006) were extracted for each field plot. They were calculated using both a 5×5 pixel ($1 \text{ m} \times 1 \text{ m}$) and 25×25 pixel ($5 \text{ m} \times 5 \text{ m}$) moving window and pixel sampling in all directions (omni-directional). These window sizes were selected following tests showing their ability to differentiate between plots of known high and low complexity (from the initial field assessment). The smaller window size was used to represent intra-object variation (within-crowns and shadows), while the large window size represented inter-object variation (crowns or canopy objects versus between-crown shadows). The GLCM textures were also expected to increase in response to increasing structural complexity, however, this turned out to be inverted. Close analysis showed that for structurally complex field plots with large openings in the overstorey that were manifested as large deep shadows in the imagery, the image texture was smoother (decreased) because both moving window sizes often included only shadow or a significant portion of nearly constant shadow brightness. As a consequence, and because image histograms for plots with large openings were somewhat bimodal, texture measures (5×5 window) were also extracted separately from canopy and shadow within each plot (i.e. using the previously described unsupervised classification as a mask).

Semivariograms were calculated for each spectral band over the whole plot in order to extract measures that have shown strong relations to forest structure (Lévesque and King, 2003; Treitz and Howarth, 2000). The range of the semivariogram, an indicator of the distance of spatial dependence, and often related to the size or scale of dominant objects in the imagery, was calculated (Curran, 1988; Johansen et al., 2007). As well, the sill was calculated as an indicator of the total structurally dependent variance in the data that was expected to respond in a manner similar to the texture measures (Johansen et al., 2007).

2.4.3. Image object variables

Finally, relating directly to field measurements of crown size, horizontal tree distribution, and canopy openness, individual objects representing branch groups, individual crowns, crown clusters and shadows were isolated in the imagery using a detection and delineation algorithm (Pouliot et al., 2005). Due to a significant crown overlap in this forest, it was not possible to delineate individual crowns. These canopy objects were converted to vector polygons and their number and size distribution were measured for each plot. In addition, a simple measure of shape complexity representing the deviation from circularity (simplest shape) (Ewers and Didham, 2007; Patton, 1975) was investigated since it was hypothesized that more irregularly shaped crowns may be associated with more complex forest structure.

2.4.4. Topographic variables

The relative position in a landscape is known to have significant effects on local forest structural conditions in terms of, for example, susceptibility to disturbance from wind (DeGayner et al., 2005; Turner and Dale, 1998) and exposure to sunlight. A raster digital elevation model (DEM) with 10 m cell size was created using a tension spline interpolator applied to an existing set of elevation points that had been generated from 25 cm pixel leaf-off stereo photos (NCC, 1998). It was evaluated using forty-two independent GPS test points and found to have a vertical RMSE of 7.52 m (Bemrose, 2006). Slope and aspect maps were derived from the DEM using standard GIS algorithms and northness (sine of aspect) and eastness (cosine of aspect) were calculated and used instead of aspect itself, which is a circular variable (Guisan et al., 1999; Lassueur et al., 2006).

A solar illumination (SI) image was also created using the sun's position at the time of image acquisition (solar zenith angle = 33.7° and solar azimuth angle = 190.2°) following the equation provided by Riano et al. (2003), as follows:

$$SI = \cos \theta_p \cos \theta_z + \sin \theta_p \sin \theta_z \cos (\phi_a - \phi_o), \quad (1)$$

where θ_p is the slope angle (i.e. slope or terrain), θ_z is the solar zenith angle, ϕ_a is the solar azimuth angle, and ϕ_o is the surface aspect angle. Since the image acquisition was close to solar noon, SI was hypothesized to be well correlated with the total illumination throughout the growing season and to provide potential explanation of some of the variance of forest structure related to productivity.

2.5. Multivariate modelling of forest structure using Redundancy Analysis

A preliminary analysis of the eighty-six image and topographic variables showed that as expected many of the image variables were correlated with one another. However, the number of variables was not reduced as is commonly done through PCA (Pasher et al., 2007) or manually through the examination of bivariate correlations (McElhinny et al., 2006). Instead, Redundancy Analysis (RDA) (Rao, 1964) was selected as the modelling method because it does not require dimensionality reduction at the input stage, allowing exploration of the variable types that were most useful for predicting a multivariate combination of the forest structure variables.

Full RDA modelling methods are provided in Pasher (2009); the following is a brief summary. RDA was used to develop a model of multivariate forest structure describing relations between multiple forest structural measurements (response variables) and multiple image and topographic variables (explanatory or predictor variables). A two-stage RDA analysis with five-hundred bootstrapped iterations (ten of fifty plots randomly excluded each time) was implemented, first in model building using forward stepwise selection and then in model validation. The resultant models were explored and a final model was selected that provided the greatest variance explanation with the fewest number of variables and the simplest set of variables, as well as the lowest % RMSE. As stated in the Introduction, this methodology is image-based. It is used to determine how much of the variance in a suite of forest structural attributes is related to the set of image variables, and, given a significant model is produced, to apply the model over the image area in predictive mapping of the linear combination of structural attributes. It does not explicitly pre-define a structural index (as in the field-based approach described in the Introduction) but instead determines a linear combination of structural variables that is significantly associated with the image and topographic data.

2.6. Mapping forest structure

As described in the Results, the RDA analysis derived a linear combination of predictor (image and topographic) variables that best explained the strongest gradient within the set of structural attributes (Legendre and Legendre, 1998). The model was then applied on a pixel-by-pixel basis across the entire study area to produce a continuous map of predicted multivariate structure. To implement this, first, standardized spatial layers representing each of the model image and topographic variables were calculated using a moving window process. The window size for each variable was the same as that used in the modelling phase. The ISODATA derived clusters of sunlit canopy and shadow were used as masks when deriving the individual spatial layers that utilized within-crown or within-shadow information. Then, the final map of predicted multivariate forest structure was calculated by multiplying the predictor variable coefficients by each of these standardized spatial layers and summing the result at each pixel across the spatial layers (i.e. application of Eq. (2) in the Results).

2.7. Validating the map of predicted multivariate forest structure

The RDA model itself was validated using the field data for the ten plots excluded in each of the five-hundred bootstrapping iterations; this is a common method used for validating biophysical models (e.g. Cohen et al., 2003; Olthof et al., 2004). This process provided validation of the continuous gradient of multivariate structure in terms of RMS error.

Validation of the output map of predicted multivariate forest structure for the whole study area using measurements of all structural variables at a large set of independent locations not used in modelling was not feasible. Instead, based on the expected use of the map to identify areas of simple and complex forest structure for further field evaluation and possible management decisions, its validation was based on assessment of these two classes only. Polygons representing areas of predicted simple and complex structure were manually identified in the map and visited in the field (with the aid of a GPS) in a random order to eliminate any a priori knowledge of the predicted structural level. These locations were selected relative to the study area as being greater than \pm two standard deviations from the map's mean value. They were spatially independent of the field plots and were in areas of the forest that had not been previously visited by the researchers. Individual structural attributes were visually assessed by two evaluators before arriving at a single conclusion with respect to the approximate structural conditions (simple, complex, or typical). Additionally, the area surrounding each location (approximately a 20 m buffer) was examined to determine if the selected locations were significantly different from their surroundings.

Seventeen complex areas (range = 450 m²–4311 m²) and eight simple areas (range = 1108 m²–11,532 m²) were validated. In addition to assessing whether they were correctly classified or not, a simple point system was used as follows: full region correctly classified (1 pt); partially correct (0.5 pts) if >50% or the area correctly classified; 0 points – the whole area was incorrectly classified.

2.8. Multiscale modelling and mapping with resampled airborne imagery

The high spatial resolution of the airborne imagery used in this study was selected based on previous experience and expected contributions from spatial and object information in the modelling. However, the collection of airborne imagery requires far greater planning and processing compared with satellite imagery due to the smaller coverage per image. Some current satellite sensors have panchromatic pixel sizes of less than 0.5 m and near future sensors will have 0.25 m pixels and multispectral pixels of less than 2 m. Therefore, the last objective of this study was to evaluate structural modelling and mapping at multiple scales. This was not meant as a comprehensive analysis of model scaling and scale dependence of variables, which is currently being examined in other ongoing research using Quickbird imagery (D. King, unpublished data), but rather an initial investigation into the scalability of the methods used in this research.

In order to accomplish this, following the above RDA procedure with the 20 cm data, the imagery was resampled to 60 cm and 1 m pixels using a 3 × 3 and 5 × 5 Gaussian filter, respectively, which approximated the point-spread function of a sensor with coarser resolution (Olthof et al., 2005). A slightly reduced set of image predictor variables ($n = 73$ as opposed to $n = 86$) was extracted from the two new lower resolution images. Some variables that were highly correlated with others that were much easier to extract were excluded from this analysis. For example, object-based percent shadow was more difficult to extract than unsupervised cluster map percent shadow, so it was excluded.

A full RDA analysis followed by mapping and validation as described above was carried out for each of the two new datasets to compare the models and resulting maps to those created using the original 20 cm imagery.

3. Results

3.1. Modelling multivariate forest structure

The RDA bootstrapping modelling process produced an in-depth and multi-faceted set of results that are described fully in Pasher (2009) and summarized here in order to focus on the final output model selected, its use in predictive structural complexity mapping

and map validation, research components of most interest to this audience. The 500 RDA models produced (all $p \leq 0.05$) were comprised of various combinations of predictor variables (Table 2). Most notably, 70% of the models included measures of within-crown texture. Topographic information and semivariogram variables (range and sill) were included in 32% and 28% of the models, respectively. Beyond that, within-crown spectral information, within-shadow spectral and spatial information and object-based information contributed moderately to the models, while full plot spectral and spatial information contributed very little.

Amongst the individual spectral variables, the only widely entered variable was average NIR reflectance within-crowns, being in 81 of 112 models that included within-crown spectral information. Of 348 models that included within-crown GLCM texture variables, 316 included the standard deviation of Homogeneity, while 110 included the average Correlation, and 96 models included both. Of the within-shadow GLCM texture variables, the standard deviation of Correlation was included in 70 out of the 90 models. The semivariogram ranges of the NIR and Green bands were included in 65 and 51 models, respectively, while the sill from any of the three bands was only included in 7 out of the 138 models with semivariogram measures. With respect to topographic information, elevation was included in 95 out of 159 models, while the variable representing illumination was included in 58 of these models. From these results, it was evident that, with this high resolution imagery, image spatial measures, in particular GLCM textures and semivariogram range, were better predictors of multivariate forest structure variability than spectral measures. In addition, within-crown and within-shadow information was more related to structure than full canopy (crowns and shadows sampled together) information, with five of the six most frequently entered variable types being within-crown or shadow (the exception being plot level semivariogram measures).

Based on the criteria given in Section 2.5, the final selected RDA model (the first RDA axis, referred to as RDA1) included five predictor variables and explained 35% of the combined variance of the field measurements (R^2 of RDA1 = 0.35, $p < 0.001$; bootstrapped RMSE = 19.9% (observed RDA1 value compared to model predicted RDA1 value)). This model was dominated by two measures of within-crown variance (Standard Deviation of GLCM Homogeneity (referred to as IM1) and Mean GLCM Correlation (IM2)), but also included two measures of within-shadow information (Mean shadow NDVI (IM3) and shadow Standard Deviation in the Green band (IM4)), as well as a small amount of explanation from elevation (IM5). Other models that provided a slightly greater explanation of variance (maximum $R^2 = 0.40$) were produced; however, they were not selected since they included semivariogram measures (range and sill variables), which were computationally intensive to calculate for all image pixels in order to produce a continuous map.

Table 2

Summarized results of RDA bootstrapping analysis in terms of sources/types of predictor variables included in the 500 models.

	# of models	% of all models
Within-crown GLCM texture	348	70
Topographic	159	32
Semivariogram range and sill	138	28
Within-crown spectral	112	22
Within-shadow first order spatial	106	21
Object-based	94	19
Within-shadow GLCM texture	90	18
Full plot GLCM texture	54	11
Subpixel fractions	50	10
Within-shadow spectral	40	8
Within-crown first order spatial	11	2
Full plot first order spatial	6	1
Full plot spectral	5	1

In the final model, IM1 and IM2 were found to be positively correlated with RDA1 ($r = 0.86$, $p < 0.001$ and $r = 0.42$, $p = 0.003$, respectively), suggesting that increasing spatial heterogeneity within the tree crowns predominantly caused by dead branches, thin crowns, and small gaps, resulted in greater within-crown GLCM texture and texture variation. IM1 had the greatest contribution and, similar to Olthof and King (2000), showed that the variation of a texture measure, as opposed to simply the mean texture, can be effective in detecting variations within tree crowns. Of note, the correlation between Mean GLCM Homogeneity and Standard Deviation of GLCM Homogeneity was 0.70 ($p < 0.001$) suggesting overlapping, but different information. An increase in the mean GLCM Correlation (IM2) in tree crowns was more difficult to interpret, as it is not a very well understood texture measure. Despite this, it has been successfully used at a variety of scales for biophysical modelling (Kayitkire et al., 2006; Wunderle et al., 2007). Van Der Sanden and Hoekman (2005) showed GLCM Correlation to be functionally equivalent to a measure of spatial autocorrelation. In this study, no measures of spatial autocorrelation within-crowns could be calculated but it was found that Correlation texture over the entire field plot was correlated with the NIR semivariogram range ($r = 0.69$, $p < 0.001$), a measure that is often associated with the size of individual objects (crown clusters and shadows) in high spatial resolution imagery (Lévesque and King, 1999). Consequently, in the RDA model, it is probably responding to increasing within-crown shadows, which are related to greater light penetration and greater vertical structural complexity.

The two predictor variables calculated from within plot shadows are thought to be related to gaps in the canopy as well as shadows caused by variable tree heights. IM3, NDVI within-shadows, is the only spectral variable entered in the model. The combination of correlations of RDA1 versus IM3 ($r = 0.30$, $p = 0.037$), and IM3 versus presence of >2 m understorey vegetation ($r = 0.33$, $p = 0.018$), suggests that IM3 was responding to increased vertical structural complexity. In addition, where tree height varies (a common indicator of increased structural complexity), overstorey crowns may be shaded by adjacent trees, thus increasing within-shadow NDVI. It must also be noted that, although the crowns of these hardwood trees are quite rounded (in comparison to conifers), small portions of each crown were shaded due to the given sun angle at the time of acquisition. These shadows could not be separated from between crown (gap) shadows. Although this was not an issue for these data acquired in a period of about 30 min at close to constant sun zenith angle, repeated acquisitions at varied sun angles could result in variations of within-shadow NDVI not related to structural variability.

The green band shadow standard deviation (IM4) was a weak contributor to the model (non-significantly correlated on its own with RDA1 ($r = -0.19$, $p = 0.192$)) and difficult to explain. Similarly, elevation (IM5) was included in the final model, however on its own it was poorly correlated with the RDA1 ($r = 0.10$, $p = 0.473$). The second RDA axis was, in fact, composed mainly of elevation variance (RDA2 correlation with elevation: $r = 0.73$, $p < 0.001$) but as presented in Pasher (2009) it was not explored further since the axis provided little explanation of the overall variance of the structural attributes.

3.2. Mapping and validation of forest structure

The first RDA axis was represented by a linear combination of predictor variables (Eq. (2)). This equation was constructed using regression or canonical coefficients for predictor variables (standardized) provided by CANOCO output (Leps and Šmilauer, 2003; ter Braak and Šmilauer, 2002). While IM4 was found to be negatively (but not significantly) correlated with RDA1 (see Section 3.1), the regression/canonical coefficient for this variable was positive (all four others were consistent). This switch in sign was attributed to the fact that in the regression equation each variable accounted for a portion of the residual variance when it was entered into the equation. IM4, although negatively related itself with RDA1, was entered into the equation

with a positive coefficient as a result of its explanation of some of the remaining residual variance.

$$\text{Predicted Forest Structure} = 0.97(IM1) + 0.40(IM2) + 0.21(IM3) + 0.35(IM4) + 0.04(IM5) \quad (2)$$

To produce a map of predicted multivariate forest structure (hereafter referred to simply as 'forest structure') (Fig. 5, with close-up example shown in Fig. 6) all the predictor layers (IM1–IM5) were standardized, resulting in values ranging from -2.8 to $+2.8$ (99% of the pixels). This map showed patterns of structure across the forest, including small patches of very complex (dark red) and very simple (dark green) structural areas (shown on the legend as greater than \pm two standard deviations from the mean). These results corresponded well to general variations seen in the forest plots and when traversing other parts of the study area. Also, as observed in the field, areas of predicted complex structures were more numerous but generally much smaller compared to the areas of predicted simple structures.

Validation of the predicted forest structure explained by the RDA model was provided above in terms of RMSE from the 500 bootstrapped iterations. In the mapping phase, forest structure was validated as a class variable using field validation. Table 3 shows a validation accuracy of 88.2% (15 of 17 regions correct) for the predicted complex class. Of the two misclassified areas, one was found to have a gully running through it that could possibly increase mutual crown shading from tree height variations, thus increasing its predicted structure level. The validation areas representing simple structure were not as well classified, with an accuracy of only 50% (4 of 8 areas). Three of the four misclassified areas, although appearing homogeneous on the map, were assessed in the field as having major changes in structure within their selected GPS boundaries (e.g. Fig. 7).

Based on the point scoring system, which accounted for partially correct classification on an areal basis, the complex regions were still 88.2% correctly classified (15 of a possible 17 points), while the simple regions were 68.8% correct (5.5 of a possible 8 points). The average accuracy of 78.5%, related well to the RDA model's RMSE found through bootstrapping (19.9%), although they are difficult to directly compare since this class-based validation focused only on the simple and complex structural conditions, and did not include the moderate conditions.

3.3. Scalability of RDA modelling and mapping

Resampling the original airborne imagery from 20 cm pixels to 60 cm and 1 m pixels resulted in an obvious loss of spatial information. Subtle brightness variations and shadows within tree crowns were greatly reduced and almost disappeared in the 1 m imagery, and individual objects such as exposed wood were almost completely lost.

Table 4 shows summary statistics for the three RDA analyses. The average adjusted R^2 values of the five-hundred models produced using the 60 cm and 1 m imagery were only slightly lower than the original 20 cm models, while the % RMSE of the models produced with the degraded imagery were slightly higher. Also of interest, the average number of predictors included in the models dropped from 3.12 (20 cm data) to 2.60 (60 cm) and 2.03 (1 m).

As the spatial resolution degraded, full plot information contributed more to models while the contributions of within-crown, within-shadow, and object-based information generally decreased. Table 5 presents the distribution of predictor variable sources/types of information included in the models. It is also worth noting that the contribution of topographic information remained stable as was expected given that the DEM was not affected by the change in resolution.

The best RDA models from the 60 cm data had between six and nine predictor variables. Of the next best models, which included only four or five variables, several had variance inflation issues. The final

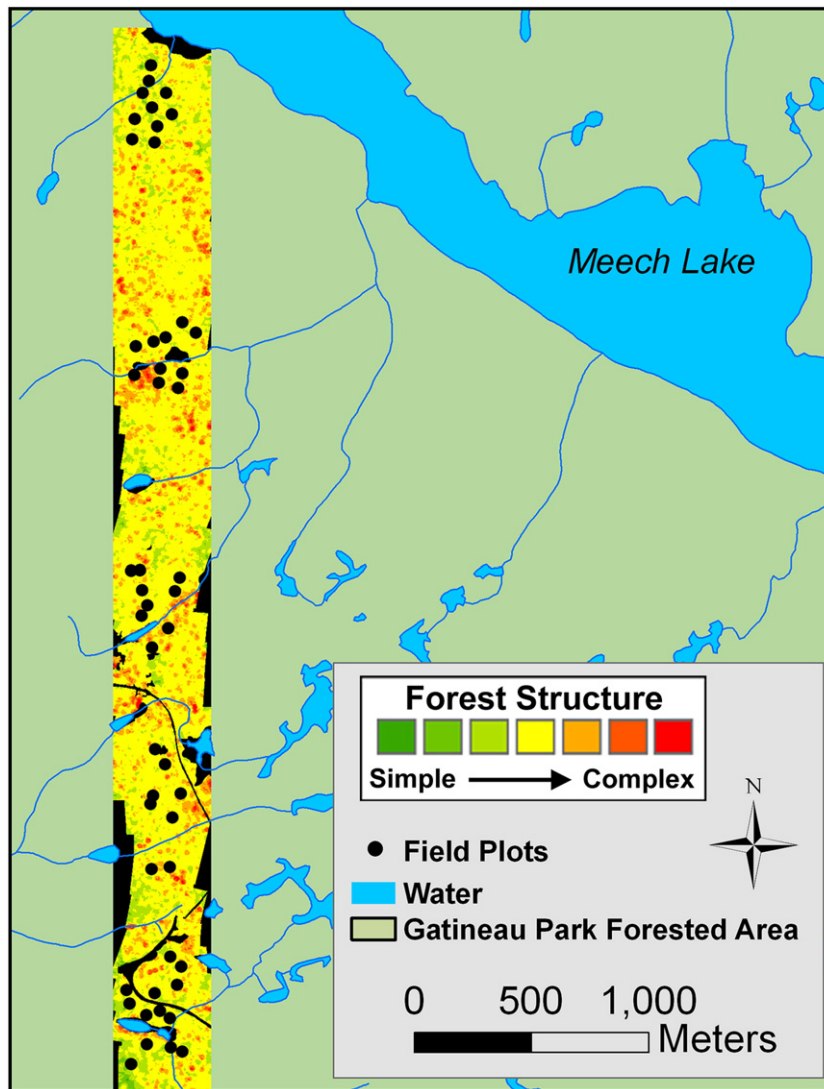


Fig. 5. Predicted forest structure mapped across the entire study area. The legend for this map, as well as all other maps presented, was created using a standard deviation classification and symbolization.

model that was selected included four predictor variables: (1) mean plot NDVI, (2) variation of unmixed sunlit fraction across the plot, (3) mean GLCM Contrast within-crowns, and (4) elevation. Its first RDA axis had an adjusted R^2 of 0.32 ($p=0.002$), providing only 3% less explanation of the variance in the field data compared to RDA1 produced from the 20 cm imagery. RDA bootstrapping produced an average RMSE of 24.9% (S.D. = 6.5%), which was approximately 5% higher than for the 20 cm model.

For the 1 m data RDA, all the best models included only three or four predictor variables. The selected model, which was the first with no variance inflation issues, contained three predictor variables: (1) variation in green reflectance across the plot, (2) plot mean GLCM Contrast, and (3) elevation. The first RDA axis (again the only significant one) had an adjusted R^2 of 0.30 ($p=0.002$) with an average RMSE of 28.4% (S.D. = 8.1%), again showing slightly less explanation of the variance in field data with a slightly higher percent error.

3.3.1. Mapping scalability and validation

The predicted structure maps produced at the coarser resolutions were directly comparable to the original map produced from the 20 cm data. Example 1 of Fig. 8 is an area that was classified similarly at all three resolutions, with only a small loss of detail in the 1 m resolution map. While this was the most prevalent condition throughout the study area,

there were also many areas where significant differences in the mapped patches of simple and complex structure were visible (Fig. 8, Example 2). Further field exploration of these areas is needed to confirm if one map was in fact more accurate than another.

In order to compare the maps to each other quantitatively, a set of two-hundred and fifty random plots (11.3 m radius circles) were created across the maps and the average predicted multivariate structure (RDA1) value within each plot was calculated. At the plot scale, the 60 cm and 1 m maps were highly correlated ($r=0.90$, $p<0.001$) while both were found to be less correlated with the 20 cm map ($r=0.66$, $p<0.001$ and $r=0.65$, $p<0.001$, respectively). Finally, a comparison of the three maps based on the independent field validation data scoring method described previously showed that the accuracy of the complex structure sites decreased from 88.2% (20 cm data) to 70.6% (60 cm data) and then to 56.3% (1 m data), while the corresponding accuracies for simple structure validation sites were 68.8%, 61.8% and 37.5%, respectively.

4. Discussion

4.1. Modelling and mapping multivariate forest structure

Forest structure modelling results were considered successful compared to previous multivariate structural modelling research that

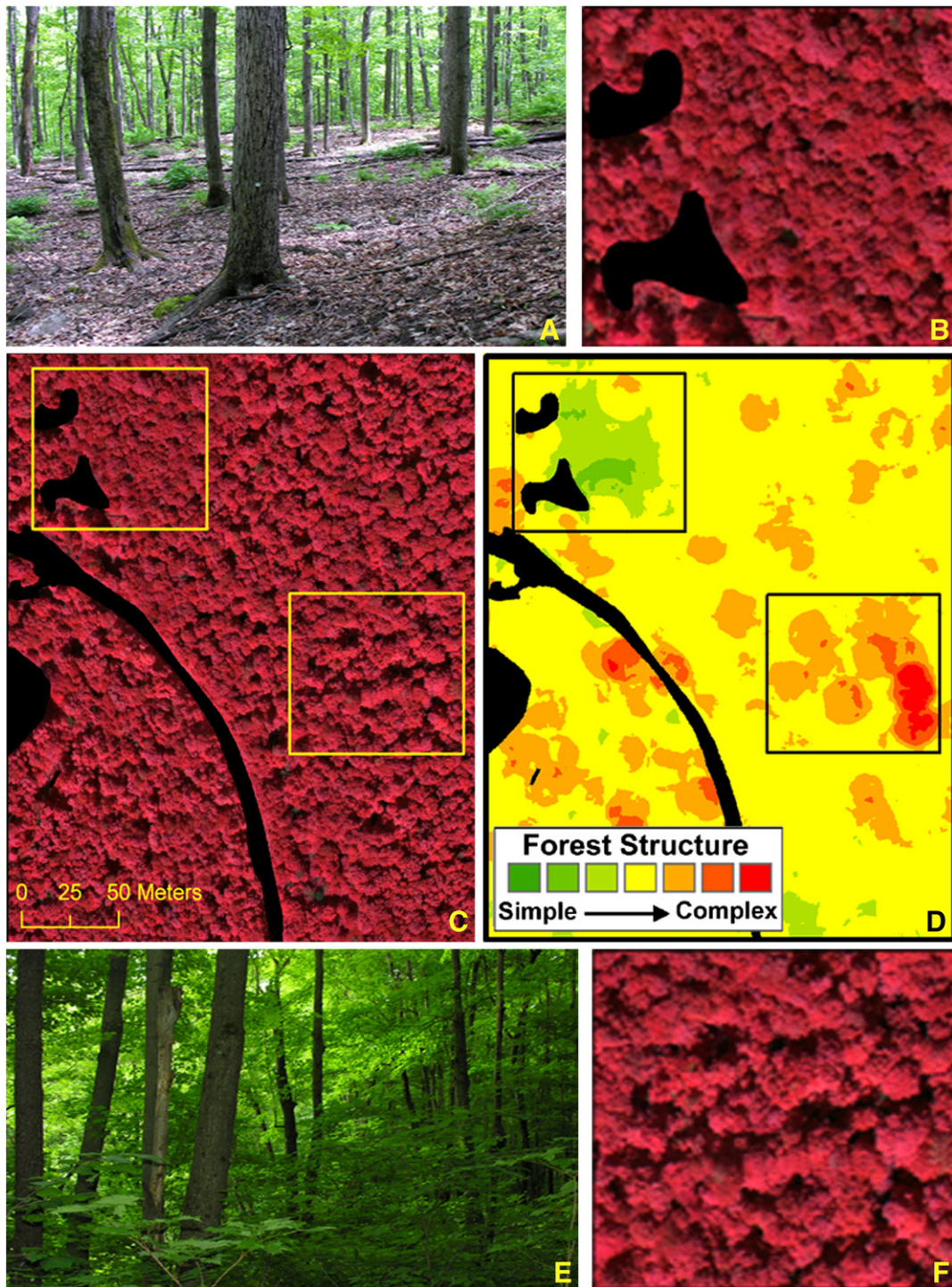


Fig. 6. Examples of mapped predicted forest structure. Masked roads and water bodies are black. (A) Field photo showing an area with simple structure, (B) a simple area at full CIR image resolution (as outlined in C and D), (C) subsection of a CIR image showing a simple area (top left box) and a complex area (middle right box), (D) map of predicted structure corresponding to the image area in C, (E) field photo showing an area with complex structure, and (F) a complex area at full CIR image resolution (as outlined in C and D).

Table 3
Results of field validation for simple and complex validation areas, presented following assessment of correct versus incorrect classification, as well as incorporating partially correct scores of 0.5.

	Complex regions		Simple regions	
	#	Points	#	Points
Correctly classified	15	15	4	4
Incorrectly classified	2	0	1	0
Partially correctly classified	0	0	3	1.5

used remotely sensed variables for predictors. While difficult to compare directly to the work by Coops and Catling (1997a,b) and Coops et al. (1998), the inclusion of the actual raw field data that was measured in the forest avoided the subjectivity and problems of repeatability inherent in qualitative scoring to measure forest structure. While others have taken the approach of modelling a pre-defined forest structure index, or score, using field-based data, the modelling presented in this paper was partially discovery-based in the sense that it explored potential image and topographic variables in order to examine relations with individual field variables, and their multivariate

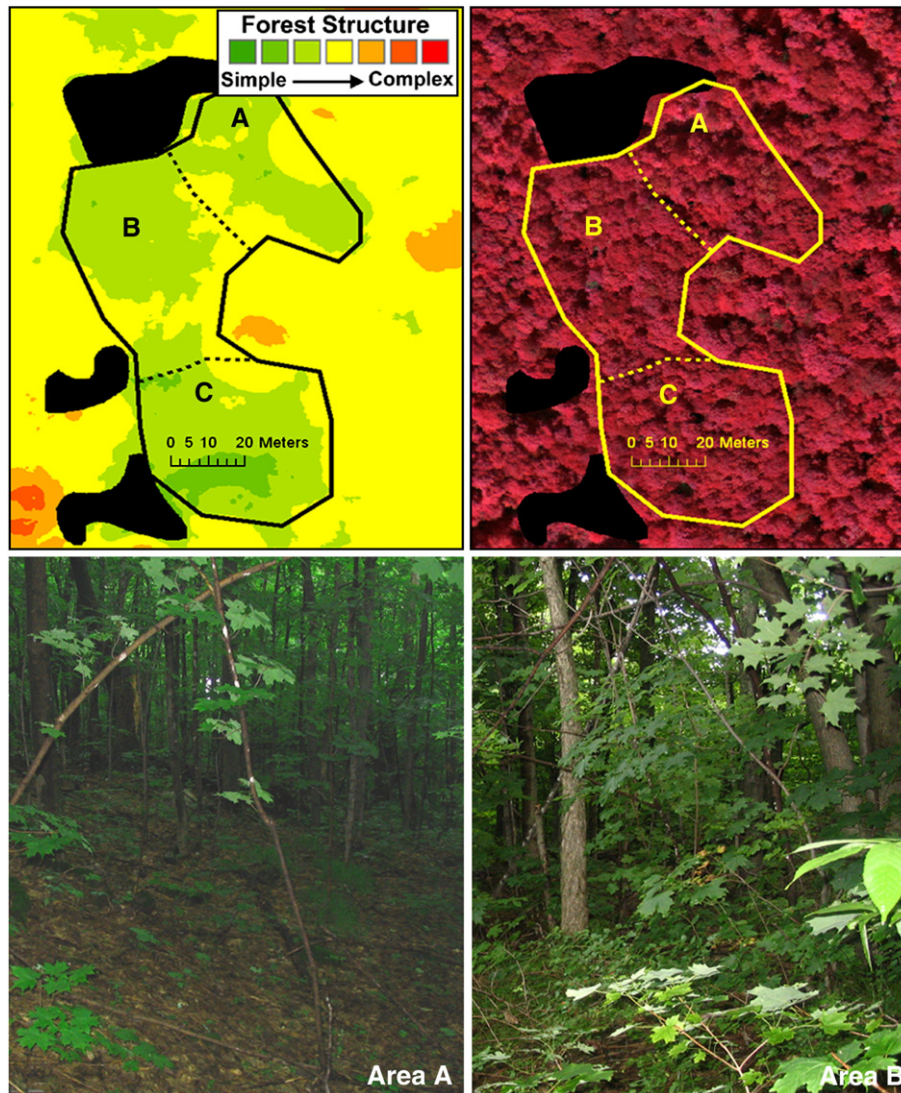


Fig. 7. Example of partially correct classification as having simple structure. The polygon (6096 m²) outlines an area mostly classified as simple in the map. Zones A and C were correct while zone B was incorrect. The field photos “Area A” and “Area B” correspond to the same areas on the map.

representation of forest structure. Future research comparing the methods and results presented here with those using a pre-defined forest structure index, using methods similar to [McElhinny et al. \(2006\)](#) would certainly be of interest to this research field. As stated earlier, [Wunderle et al. \(2007\)](#) took this approach, but used PCA of the field data to first define a field-based structural index. In modelling of this index against SPOT spectral and spatial data, they found a high correspondence between predicted and modelled structural complexity

Table 4

Summary statistics calculated from models produced from the first phase of RDA bootstrapping using predictor variables extracted from 60 cm and 1 m imagery independently.

		Adjusted R^2	# of predictors	% RMSE
20 cm	Average	0.29	3.12	25.6
	Minimum	0.17	1.00	17.6
	Maximum	0.48	14.00	38.3
60 cm	Average	0.28	2.60	28.7
	Minimum	0.19	1.00	19.7
	Maximum	0.46	16.00	36.5
1 m	Average	0.25	2.03	30.8
	Minimum	0.07	1.00	23.3
	Maximum	0.37	10.00	51.4

($R^2=0.79$), with image predictor variables including two texture measures calculated from the gray-level co-occurrence matrix, along with a single spectral variable.

Using an image-based approach as in the current research, [Cosmopoulos and King's \(2004\)](#) forest structure index (FSI) was produced through a pseudo-RDA analysis, with three stages: PCA of the field and image data followed by CCA using a subset of the principal components to reduce dimensionality, followed by stepwise regression of the original image variables against the first field canonical variate (FSI). At each stage some variance in the original data was lost, resulting in a final model explanation of 26% of the original variance of the raw field data. The complicated nature of such an analysis in terms of the interpretation required at each step supports the use of RDA for this type of multivariate modelling. Similar to the results of this research, the FSI presented by [Cosmopoulos and King \(2004\)](#) used mostly spatial image information (4 out of the 5 predictor variables). The variation of GLCM texture was the first variable entered into the FSI regression model, accounting for ~62% of the total explained variance (i.e. 62% of the 26% variance in the field data accounted for by the model). Similarly, a multiple regression using RDA1 from the current research as the dependent variable against the five predictor variables (IM1–IM5) also entered the variation of GLCM texture as the most important predictor variable, and it accounted for ~73% of the overall explained variance (i.e.

Table 5

Types of predictor variables included in the 500 RDA models produced through bootstrapping with the three scales of imagery. The top three contributors for each resolution are bolded to highlight major differences.

	% of models		
	20 cm	60 cm	1 m
Within-crown GLCM texture	70	25	16
Topographic	32	29	28
Semivariogram range and sill	28	6	14
Within-crown spectral	22	12	2
Within-shadow 1st order spatial	21	2	3
Object-based	19	3	1
Within-shadow GLCM texture	18	5	14
Full plot GLCM texture	11	73	16
Subpixel fractions	10	23	42
Within-shadow spectral	8	1	1
Within-crown 1st order spatial	2	4	2
Full plot 1st order spatial	1	7	44
Full plot spectral	1	18	6

73% of the 35% variance in the field data accounted for by the model) in predicted forest structure. In the other two studies found that used RDA for forest structure modelling, spatial information was not included. Sampson et al. (2001) used only a few spectral indices derived from airborne imagery and found weak relations. de la Cueva (2008) modelled forest structure using Landsat spectral information and topographic variables, with a maximum of only 24% explanation when combining both the first and second RDA axes. The lack of spatial information, which was not available at the plot scale using Landsat imagery, was a major limitation of their research.

Other than IM5 (elevation), all variables included in RDA1 from the 20 cm data model represented within-crown and within-shadow information, as opposed to information extracted across the entire plot. It had originally been hypothesized that the presence of canopy gaps in more complex areas would result in lower plot average reflectance and greater image spatial variability compared to more structurally simple areas. However, variables representing full plot spectral information (i.e. extracted over the canopy and including shadows and crowns) were only included in five out of the five-hundred models. Furthermore, comparing the average plot reflectance of the three spectral variables to RDA1 showed no relations (NIR: $r = -0.19$ ($p = 0.19$), Red: $r = -0.15$ ($p = 0.31$), and Green: $r = -0.11$ ($p = 0.50$)). As well, full plot GLCM textures (i.e. spatial information) were only included in 54 of the 500 models.

The predicted forest structure (RDA1) was interpreted based on correlations with the individual field variables. In general more complex structures were associated with increasing canopy openness and understorey vegetation (>2 m), decreasing low ground vegetation (0–50 cm), increasing snag size (average snag dbh), increasing dead basal area, an increasing number of CWD pieces, increasing overstorey tree size and number of “large” trees, and a decrease of the number of those trees (number of overstorey trees and live basal area) (full table of correlations included in Pasher (2009)). The individual field variables had originally been selected following an extensive literature review of potential structural variables in order to represent the abundance and variability of different horizontal and vertical aspects of forest structure. Most notably, the number of snags was uncorrelated with RDA1 and suggested that not all of the field-based variance of structure could be modelled using an image-based

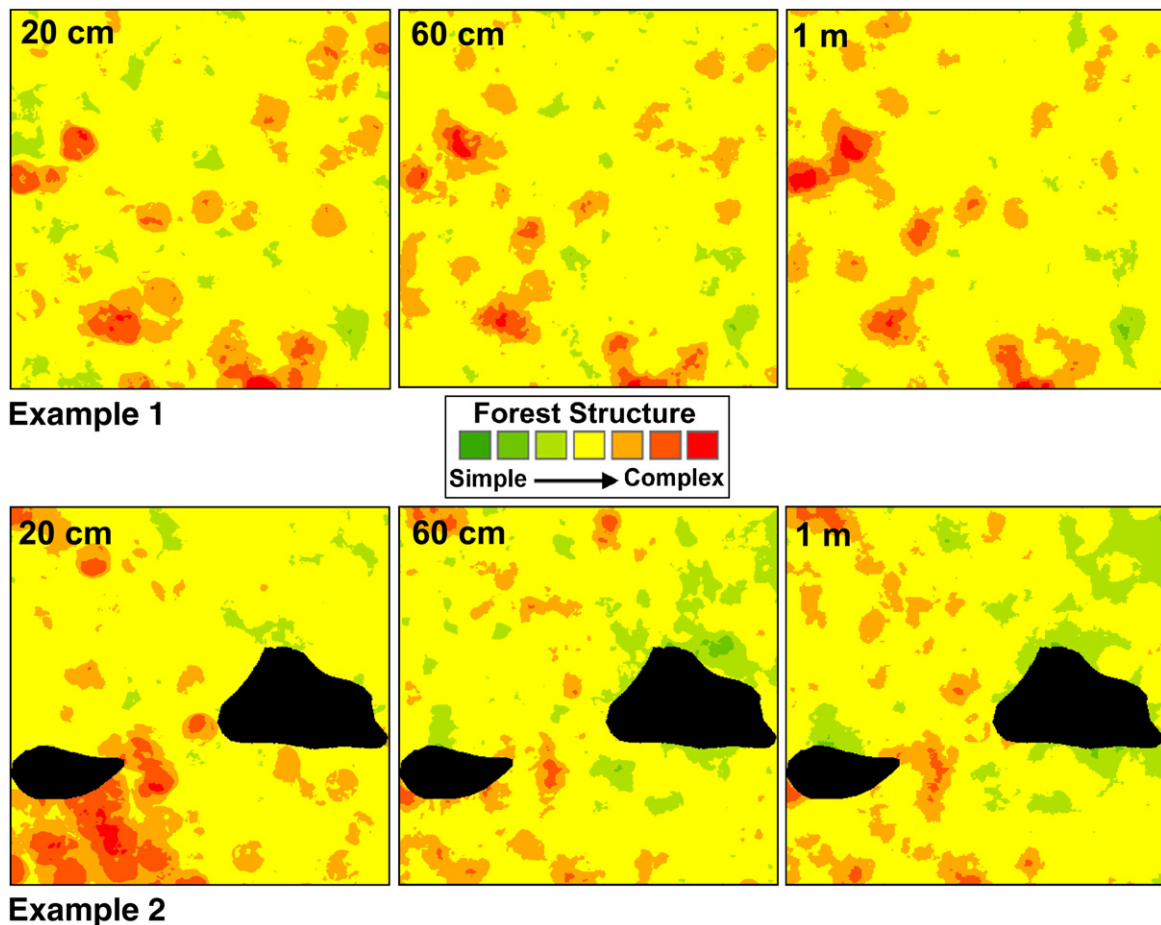


Fig. 8. Two example regions (each 250 m × 250 m) extracted from the three different resolution maps of predicted forest structure. Example 1 is an area that corresponded well between the different resolutions; Example 2 showed significant differences. Masked water bodies appear as black.

approach (Pasher, 2009), providing justification for associated research by the authors investigating the detection and mapping of dead wood in a temperate hardwood forest (Pasher and King, 2009).

The second objective of this research was to map predicted forest structure. The inherent structure of the RDA was fully exploited in order to develop an empirical model that was used for predictive mapping of the forest structure. The map accuracies of 88% (complex structural areas) and 69% (simple structural areas) are suitable for targeting areas for further study or management (e.g. for conservation, or remediation, respectively). Errors in predicted structure across the forest may occur in locations where structural conditions do not follow the typical trend of increasing overhead canopy openness and heterogeneity associated with sub-canopy vegetation development. This is a result of the model's sensitivity primarily to changes in the upper canopy and to a lesser extent to increased reflectance from tall understorey vegetation in gap shadows, which are directly measurable in the imagery, as opposed to sub-canopy changes that cannot be directly measured.

4.2. Scalability of structural modelling and mapping

Model scaling tests showed significant changes in the types of information included in the coarser resolution models. Degrading the imagery resulted in a loss of spatial information, and within-crown shadows began to disappear in the 60 cm imagery, while many of the significant canopy gaps visible in the original 20 cm imagery were almost completely lost in the 1 m imagery. The types of variables included in the RDA models changed with scale from within-crown and shadow variables to plot level variables for coarser resolution models, a result directly attributable to the mixing of information within pixels. Within-crown GLCM spatial information was included in only 25% and 16% of the new models, and within-crown spectral information was included in only 12% and 2% for the 60 cm and 1 m models, respectively. Instead, full plot spatial information contributed to 73% of models produced with 60 cm data, and, interestingly, at the 1 m spatial resolution, plot level first order spatial information was included in the models, suggesting that second order textural information was no longer detectable within objects at this scale. As well, subpixel fractions were found to be important for models produced from the 1 m imagery, contributing to 42% of the models. These results suggest that information within mixed pixels at the coarser scale may be accessible through unmixing and aid such modelling with coarser resolution airborne or satellite imagery.

The amount of structural variance explained decreased by only 3% and 5% for the 60 cm and 1 m models, respectively, from the original 20 cm model, and the RMSE associated with the models increased from 19.9% (20 cm) to 24.9% and 28.4%, respectively. Validation of the coarser resolution maps using the independent field validation sites showed overall accuracy to be 63.4% (60 cm) and 49.7% (1 m), compared to 78.5% accuracy for the 20 cm imagery. The large discrepancy between model and map accuracies was unexplainable and further field exploration may be required. Perhaps as found by Lévesque and King (2003), who analyzed airborne imagery with 25 cm, 50 cm and 1 m resolutions, the mid resolution (50 cm in that study case and 60 cm here) may provide the best compromise between modelling within-crown and shadow information with low image coverage and modelling plot – canopy level information with coarser resolution and larger image coverage. This is the subject of ongoing research with high resolution satellite imagery.

4.3. Potential application and further research

The methods and results presented in this manuscript are intended for local scale forest management. The actual models and specific relationships derived could have been applied across a larger area of the Gatineau Park had larger image coverage been acquired as the general forest structure and composition variability in the rest of the park is not

significantly different from the study area. However, the derived model variables and coefficients are not expected to be transferable over large distances to different forest ecosystems. Instead, it is the methods that are transferable. With a new set of imagery and field (ie. for training) plots the same methods could be applied to other hardwood forests to derive a similar type of multivariate forest structure model. Further, mapping forest structure across larger areas than that of this study is limited if high spatial resolution imagery is used on its own, even though camera systems do exist that provide much greater coverage in a single frame compared to the camera used in this research. In particular, since NIR brightness was not found to be as important as image spatial characteristics, large format color cameras with swaths on the order of 4000–6000 pixels could be used to derive textures and other spatial information, but with the possibility that sun angle–view angle issues may arise if wall-to-wall mapping is attempted. These types of issues, for the most part, were controlled in this analysis. As an alternative, applying the methods across larger areas for forest management could be sample-based, involving a set of monitoring locations. These areas could be selected manually on the ground to represent different conditions, perhaps coinciding with existing forest inventory plots, with the necessary field data already acquired. The targeted areas could then be covered by a several high spatial resolution images, using only the central portion of each image to limit view angle effects. The use of very high spatial resolution imagery is preferable, even if it only provides sample-based spatial coverage, as within-crown and within-shadow information was shown to be better for modelling and mapping forest structure than canopy level image information derived from coarser resolution imagery. However, high resolution satellite imagery with greater spatial coverage could provide less precise modelling and mapping (e.g. with 2–3 structural classes) using canopy variables across larger areas. A similar sampling approach would still be required as a result of acquisition costs and the viewing geometry between multiple photos (Wulder et al., 2008).

The structural modelling approach presented in this research was based on high spatial resolution digital airborne imagery, however, it is not meant to be a sole alternative to other sensors as combination with lidar, radar or other data types could enhance such multivariate forest structure modelling. Specifically, lidar has been successfully used to model individual structural attributes at a variety of scales in predominantly coniferous forests, (e.g. Breidenbach et al., 2008; Lefsky et al., 2002, 2005; Popescu et al., 2004) as well as deciduous forests (e.g. Lim et al., (2003) in a forest of similar composition to that of this study). Popescu et al. (2004) found leaf-off lidar to perform not as well in deciduous forest as in coniferous forest while Anderson et al. (2008) found a combination of lidar and airborne hyperspectral (AVIRIS) imagery with a pixel size of about 16–17 m to be better than either sensor type alone for modelling of individual structural attributes. Perhaps the most similar analysis to this research is that of Lefsky et al. (2005) who modelled a multivariate combination of structural attributes with lidar in coniferous forests of Washington and Oregon, U.S.A. Canonical Correlation Analysis (CCA) was applied to explore relations between 29 lidar variables and 18 structural attributes. The first two canonical axes explained 61% and 15% of the field data variance, respectively.

Based on these findings, combining leaf-on or leaf-off lidar with high resolution airborne imagery should improve predictive forest structure models. In the future, high resolution satellite optical and lidar data will provide much larger spatial coverage with sufficiently narrow view angles to apply this multivariate structural modelling and mapping methodology over larger areas.

5. Conclusions

This research has presented new evidence that high resolution image spectral, spatial, and object-based information combined with topographic information are useful as complementary inputs to

multivariate modelling of forest structure. The methods presented here were designed based on earlier work involving field-based complexity indices, as well as image-based modelling involving linear regression, canonical correlation analysis, and Redundancy Analysis (RDA). The use of RDA resulted in a model representing a significant portion of the variance in multiple forest structural attributes. While only 35% of the field variance was explained by the model, validation showed this to be sufficient for mapping general structural conditions. The results of this research highlight the importance of using very high spatial resolution imagery in order to extract within-crown and within-shadow information. Based on testing using simulated coarser resolution imagery, high resolution satellite sensors may potentially be useful for carrying out such modelling and mapping, however further testing is required.

This research used RDA to not only examine relations between field and image variables on a point and plot-based scale, but to predict and continuously map multivariate forest structure across a study area. This approach has the potential in forest management for damage, disturbance and habitat mapping, amongst other applications where the spatial pattern of structure in a forest may aid in understanding of forest processes. While this paper focused on the modelling–mapping–validation process, as previously mentioned, a companion manuscript has been submitted, which presents detailed field methods, RDA modelling, and interpretation within an ecologic context (also available in Pasher (2009)).

Acknowledgements

This research was funded by an NSERC Discovery Grant to D. King. The Canada Foundation for Innovation, the Ontario Innovation Trust, the National Wildlife Research Centre and private sources funded Carleton University's Geomatics and Landscape Ecology Laboratory (GLEL), which provided all the necessary field equipment and data processing infrastructure used in this research. The authors are grateful to the NCC for access to Gatineau Park and for providing geospatial data used in this research. Many thanks to C. Czerwinski for his extensive help in the field, as well as M. Leni, V. Torontow, and R. Bemrose. The continuous feedback and advice of I. Olthof (Canada Centre for Remote Sensing), E. Humphreys (Geography, Carleton University) and J. Kerr (Biology, University of Ottawa) has been greatly appreciated. Many thanks to N. Walsworth, D. Patterson, and E. Seed for technical support and manuscript editing. Finally, the intensive RDA modelling support and advice of R. Proulx (currently at the Max Planck Institute, Germany) are greatly appreciated.

References

- Anderson, J. E., Plourde, L. C., Martin, M. E., Braswell, B. H., Smith, M. -L., Dubayah, R. O., Hofton, M. A., & Blair, J. B. (2008). Integrating waveform Lidar with hyperspectral imagery for inventory of a northern temperate forest. *Remote Sensing of Environment*, 112(4), 1856–1870.
- Bemrose, R.K. 2006. Impacts of radiometric corrections on empirical modelling of biophysical variables with airborne multispectral digital camera imagery. MSc Thesis, Department of Geography and Environmental Studies, Carleton University, Ottawa, Ontario. 150 pp.
- Breidenbach, J., Koch, B., Kandler, G., & Kleusberg, A. (2008). Quantifying the influence of slope, aspect, crown shape and stem density on the estimation of tree height at plot level using Lidar and InSAR data. *International Journal of Remote Sensing*, 29(5), 1511–1536.
- Bruniquel-Pinel, V., & Gastellu-Etchegorry, J. P. (1998). Sensitivity of texture of high resolution images of forest to biophysical and acquisition parameters. *Remote Sensing of Environment*, 65(1), 61–85.
- Butson, C. R., & King, D. J. (1999). Semivariance analysis of forest structure and remote sensing data to determine an optimal sample plot size. *Proceedings of the 4th international airborne remote sensing conference and exhibition/21st Canadian symposium on remote sensing, June 21–24, Ottawa, Ontario, Vol. II.* (pp. 155–162).
- Butson, C. R., & King, D. J. (2006). Lacunarity analysis to determine optimum extents for sample-based spatial information extraction from high-resolution forest imagery. *International Journal of Remote Sensing*, 27(1–2), 105–120.
- Cohen, W. B., Maierberger, T. K., Gower, S. T., & Turner, D. P. (2003). An improved strategy for regression of biophysical variables and Landsat ETM+ data. *Remote Sensing of Environment*, 84(4), 561–571.
- Coops, N. C., & Catling, P. C. (1997). Predicting the complexity of habitat in forests from airborne videography for wildlife management. *International Journal of Remote Sensing*, 18(12), 2677–2682.
- Coops, N. C., & Catling, P. C. (1997). Utilising airborne multispectral videography to predict habitat complexity in eucalypt forests for wildlife management. *Wildlife Research*, 24, 691–703.
- Coops, N. C., Culvenor, D., Preston, R., & Catling, P. C. (1998). Procedures for predicting habitat and structural attributes in eucalypt forests using high spatial resolution remotely sensed imagery. *Australian Forestry*, 61(4), 244–252.
- Cosmopoulos, P., & King, D. J. (2004). Temporal analysis of forest structural condition at an acid mine site using multispectral digital camera imagery. *International Journal of Remote Sensing*, 25(12), 2259–2275.
- Curran, P. (1988). The semivariogram in remote sensing: An introduction. *Remote Sensing of Environment*, 24(3), 493–507.
- de la Cueva, A. V. (2008). Structural attributes of three forest types in central Spain and Landsat ETM plus information evaluated with redundancy analysis. *International Journal of Remote Sensing*, 29(19), 5657–5676.
- DeGayer, E. J., Kramer, M. G., Doerr, J. G., & Robertsen, M. J. (2005). Windstorm disturbance effects on forest structure and black bear dens in southeast Alaska. *Ecological Applications*, 15(4), 1306–1316.
- Ewers, R. M., & Didham, R. K. (2007). The effect of fragment shape and species' sensitivity to habitat edges on animal population size. *Conservation Biology*, 21(4), 926–936.
- Fernandes, R., Butson, C., Leblanc, S., & Latifovic, R. (2003). Landsat-5 TM and Landsat-7 ETM+ based accuracy assessment of leaf area index products for Canada derived from SPOT-4 VEGETATION data. *Canadian Journal of Remote Sensing*, 29(2), 241–258.
- Franklin, S. E., Hall, R. J., Moskal, L. M., Maudie, A. J., & Lavigne, M. B. (2000). Incorporating texture into classification of forest species composition from airborne multispectral images. *International Journal of Remote Sensing*, 21(1), 61–79.
- Gastellu-Etchegorry, J. P., Demarez, V., Pinel, V., & Zagolski, F. (1996). Modeling radiative transfer in heterogeneous 3-D vegetation canopies. *Remote Sensing of Environment*, 58, 131–156.
- Geospatial Systems Inc. 2007. <http://www.geospatialsystems.com/>.
- Guisan, A., Weiss, S. B., & Weiss, A. D. (1999). GLM versus CCA spatial modelling of plant species distribution. *Plant Ecology*, 143(1), 107–122.
- Hall, R. J., Davidson, D. P., & Peddle, D. R. (2003). Ground and remote estimation of leaf area index in Rocky Mountain forest stands, Kananaskis, Alberta. *Canadian Journal of Remote Sensing*, 29(3), 411–427.
- Hall, R. J., Skakun, R. S., Arsenault, E. J., & Case, B. S. (2006). Modeling forest stand structure attributes using Landsat ETM+ data: Application to mapping of aboveground biomass and stand volume. *Forest Ecology and Management*, 225(1–3), 378–390.
- Haralick, R. M., Shanmugan, K., & Dinstein, I. (1973). Textural features for image classification. *IEEE Transactions on Systems, Man, and Cybernetics*, SMC-3, 610–621.
- Jakubauskas, M. E. (1996). Canonical correlation analysis of coniferous forest spectral and biotic relations. *International Journal of Remote Sensing*, 17(12), 2323–2332.
- Johansen, K., & Phinn, S. (2006). Linking riparian vegetation spatial structure in Australian tropical savannas to ecosystem health indicators: Semi-variogram analysis of high spatial resolution satellite imagery. *Canadian Journal of Remote Sensing*, 32(3), 228–243.
- Johansen, K., Coops, N. C., Gergel, S. E., & Stange, Y. (2007). Application of high spatial resolution satellite imagery for riparian and forest ecosystem classification. *Remote Sensing of Environment*, 110(1), 29–44.
- Kayitakire, F., Hamel, C., & Defourny, P. (2006). Retrieving forest structure variables based on image texture analysis and Ikonos-2 imagery. *Remote Sensing of Environment*, 102(3–4), 390–401.
- King, D. J., Olthof, I., Pellikka, P. K. E., Seed, E. D., & Butson, C. (2005). Modelling and mapping forest ice storm damage using remote sensing and environmental data. *Natural Hazards, Special Issue on Remote Sensing*, 35(3), 321–342.
- Lassueur, T., Joost, S., & Randin, C. F. (2006). Very high resolution digital elevation models. Do they improve models of plant species distribution? *Ecological Modelling*, 198(1–2), 139–153.
- Leblanc, S. G., & Chen, J. M. (1998). Applications of the 4-scale radiative-transfer model in the remote sensing of boreal forests. *Proceedings IEEE International Geoscience and Remote Sensing Symposium (IGARSS) 1998* (pp. 1484–1486).
- Lefsky, M. A., Cohen, W. B., Parker, G. G., & Harding, D. J. (2002). Lidar remote sensing for ecosystem studies. *BioScience*, 52(1), 19–30.
- Lefsky, M. A., Cohen, W. B., & Spies, T. A. (2001). An evaluation of alternate remote sensing products for forest inventory, monitoring, and mapping of Douglas-fir forests in western Oregon. *Canadian Journal of Remote Sensing*, 31(1), 78–87.
- Lefsky, M. A., Hudak, A. T., Cohen, W. B., & Acker, S. A. (2005). Patterns of covariance between forest stand and canopy structure in the Pacific Northwest. *Remote Sensing of Environment*, 95(4), 517–531.
- Legendre, P., & Legendre, L. (1998). Numerical ecology, 2nd English edition. Amsterdam: Elsevier Science BV 870 pp.
- Leps, J., & Šmilauer, P. (2003). Multivariate analysis of ecological data using CANOCO. Cambridge, UK: Cambridge University Press 269 pp.
- Lévesque, J., & King, D. J. (1999). Airborne digital camera image semivariance for evaluation of forest structural damage at an acid mine site. *Remote Sensing of Environment*, 68(2), 112–124.
- Lévesque, J., & King, D. J. (2003). Spatial analysis of radiometric fractions from high-resolution multispectral imagery for modelling individual tree crown and forest canopy structure and health. *Remote Sensing of Environment*, 84(4), 589–602.
- Li, X., & Strahler, A. H. (1992). Geometric-optical bi-directional reflectance modeling of discrete crown vegetation canopy: Effect of crown shape and mutual shadowing. *IEEE Transactions on Geoscience and Remote Sensing*, 30(2), 276–292.
- Lim, K., Treitz, P., Baldwin, K., Morrison, I., & Green, J. (2003). Lidar remote sensing of biophysical properties of tolerant northern hardwood forests. *Canadian Journal of Remote Sensing*, 29(5), 658–678.

- Lopoukhine, N. (1974). The forests and associated vegetation of Gatineau Park, Quebec. *Forest Management Institute Information Report FMR-X-58, Study FM-72. Ottawa, Ontario.*
- McElhinny, C., Gibbons, P., & Brack, C. (2006). An objective and quantitative methodology for constructing an index of stand structural complexity. *Forest Ecology and Management*, 235(1–3), 54–71.
- McElhinny, C., Gibbons, P., Brack, C., & Bauhus, J. (2005). Forest and woodland stand structural complexity: Its definition and measurement. *Forest Ecology and Management*, 218(1–3), 1–24.
- Meyer, P., Itten, K. I., Kellenberger, T., Sandmeier, S., & Sandmeier, R. (1993). Radiometric corrections of topographically induced effects on Landsat TM data in an alpine environment. *Journal of Photogrammetry and Remote Sensing*, 48(4), 17–28.
- National Capital Commission (NCC). (1998). Digital elevation data for Gatineau Park. Ottawa, Ontario: NCC.
- National Capital Commission (NCC). (2004). Digital orthophotos. Ottawa, National Capital Commission.
- National Capital Commission (NCC). (2005). Gatineau Park master plan http://www.ncc-ccn.gc.ca/data/2/rec_docs/1768_Master_Plan_e.pdf
- Nelson, R. F., Hyde, P., Johnson, P., Emessiene, B., Imhoff, M. L., Campbell, R., & Edwards, W. (2007). Investigating Radar–Lidar synergy in a North Carolina pine forest. *Remote Sensing of Environment*, 110(1), 98–108.
- Neumann, M., & Starlinger, F. (2001). The significance of different indices for stand structure and diversity in forests. *Forest Ecology and Management*, 145(1–2), 91–106.
- Nielsen, M.O. 2004. True orthophoto generation. MSc Thesis, Department of Informatics and Mathematical Modelling, Technical University of Denmark, Lyngby, Denmark. 142 pp.
- Olthof, I., & King, D. J. (1997). Evaluation of textural information in airborne CIR digital camera imagery for estimation of forest stand leaf area index. *Proceedings of the first North American symposium on small formation aerial photography, Oct. 14–17 1997, Cloquet, MN* (pp. 154–164).
- Olthof, I., & King, D. J. (2000). Development of a forest health index using multispectral airborne digital camera imagery. *Canadian Journal of Remote Sensing*, 26, 166–176.
- Olthof, I., King, D. J., & Lautenschlager, R. A. (2004). Mapping deciduous forest ice storm damage using Landsat and environmental data. *Remote Sensing of Environment*, 89(4), 484–496.
- Olthof, I., Pouliot, D., Fernandes, R., & Latifovic, R. (2005). Landsat-7 ETM+ radiometric normalization comparison for northern applications. *Remote Sensing of Environment*, 95(3), 388–398.
- Omari, K., White, H. P., & Staenz, K. (2009). An enhanced description of multiple scattering within the FLAIR model using the photon re-collision probability approach. *IEEE Transactions on Geosciences and Remote Sensing*, 47(8), 2931–2941.
- Pasher, J. 2009. Forest structural complexity in a temperate hardwood forest: A geomatics approach to modelling and mapping indicators of habitat and biodiversity. PhD Thesis, Department of Geography and Environmental Studies, Carleton University, Ottawa, Ontario. 220pp.
- Pasher, J., & King, D. J. (2009). Mapping dead wood distribution in a temperate hardwood forest using high resolution airborne imagery. *Forest Ecology and Management*, 258(7), 1536–1548.
- Pasher, J., King, D. J., & Lindsay, K. (2007). Modelling and mapping potential hooded warbler (*Wilsonia citrina*) habitat using remotely sensed imagery. *Remote Sensing of Environment*, 107(3), 471–483.
- Patton, D. R. (1975). A diversity index for quantifying habitat edge. *Wildlife Society Bulletin*, 3, 171–173.
- Peddle, D. R., Hall, F. G., & LeDrew, E. F. (1999). Spectral mixture analysis and geometric-optical reflectance modelling of boreal forest biophysical structure. *Remote Sensing of Environment*, 67, 288–297.
- Peddle, D. R., Johnson, R. L., Cihlar, J., & Latifovic, R. (2004). Large area forest classification and biophysical parameter estimation using the 5-scale canopy reflectance model in Multiple-Forward Mode. *Remote Sensing of Environment*, 89(2), 252–263.
- Pellikka, P. K. E. (1998). Development of correction chain for multispectral airborne video camera data for natural resource assessment. *Fennia*, 176, 1–110.
- Pellikka, P. K. E., Seed, E. D., & King, D. J. (2000). Modelling deciduous forest ice storm damage using CIR aerial imagery and hemispheric photography. *Canadian Journal of Remote Sensing*, 26(5), 394–405.
- Pickup, G., Chewings, V. H., & Pearce, G. (1995). Procedures for correcting high resolution airborne video imagery. *International Journal of Remote Sensing*, 16(9), 1647–1662.
- Popescu, S. C., Wynne, R. H., & Scrivani, J. A. (2004). Fusion of small-footprint Lidar and multispectral data to estimate plot-level volume and biomass in deciduous and pine forests in Virginia, USA. *Forest Science*, 50(4), 551–565.
- Pouliot, D. A., King, D. J., & Pitt, D. G. (2005). Development and evaluation of an automated tree detection–delineation algorithm for monitoring regenerating coniferous forests. *Canadian Journal of Forest Research*, 35(10), 2332–2345.
- Rao, C. R. (1964). The use and interpretation of principal component analysis in applied research. *Sankha*, 26, 329–358.
- Riano, D., Chuvieco, E., Salas, J., & Aquado, I. (2003). Assessment of different topographic corrections in Landsat-TM data for mapping vegetation types. *IEEE Transactions on Geoscience and Remote Sensing*, 41(5), 1056–1061.
- Richter, R. (2005). *Atmospheric/topographic correction for satellite imagery (ATCOR-2/3 User Guide Version 6)* (pp. 26–27). Wessling, Germany: German Aerospace Centre.
- Sampson, P. H., Treitz, P. M., & Mohammed, G. H. (2001). Remote sensing of forest condition in tolerant hardwoods: An examination of spatial scale, structure and function. *Canadian Journal of Remote Sensing*, 27(3), 232–246.
- Seed, E. D., & King, D. J. (2003). Shadow brightness and shadow fraction relations with effective LAI: Importance of canopy closure and view angle in mixedwood boreal forest. *Canadian Journal of Remote Sensing*, 29(3), 324–335.
- Soenen, S. A., Peddle, D. R., & Coburn, C. A. (2005). SCS + C: A modified sun-canopy-sensor topographic correction in forested terrain. *IEEE Transactions on Geoscience and Remote Sensing*, 43(9), 2148–2159.
- Spies, T. A., & Franklin, J. F. (1991). The structure of natural young, mature, and old-growth Douglas-Fir forests in Oregon and Washington. In K. B. Aubry, M. H. Brookes, J. K. Agee, R. G. Anthony, & J. F. Franklin (Eds.), *Wildlife and vegetation of unmanaged Douglas-Fir forests* (pp. 91–109). Portland, Oregon: USDA Forest Service.
- Teillet, P. M., Guindon, B., & Goodenough, D. G. (1982). On the slope-aspect correction of multispectral scanner data. *Canadian Journal of Remote Sensing*, 8(2), 84–106.
- ter Braak, C. J. F., & Šmilauer, P. (2002). *CANOCO reference manual and CanoDraw for Windows. User's guide: Software for Canonical Community Ordination* (v. 4.5). Ithaca, NY: Microcomputer Power 500 pp.
- Treitz, P., & Howarth, P. (2000). High spatial resolution remote sensing data for forest ecosystem classification: An examination of spatial scale. *Remote Sensing of Environment*, 72(3), 268–289.
- Turner, M. G., & Dale, V. H. (1998). Comparing large infrequent disturbances: What have we learned? *Ecosystems*, 1(6), 493–496.
- Van Der Sanden, J. J., & Hoekman, D. H. (2005). Review of relationships between grey-tone co-occurrence, semivariance, and autocorrelation based image texture analysis approaches. *Canadian Journal of Remote Sensing*, 31(3), 207–213.
- Wulder, M. (1998). Optical remote-sensing techniques for the assessment of forest inventory and biophysical parameters. *Progress in Physical Geography*, 22(4), 449–476.
- Wulder, M. A., LeDrew, E. F., Franklin, S. E., & Lavigne, M. B. (1998). Aerial image texture information in the estimation of northern deciduous and mixed wood forest leaf area index (LAI). *Remote Sensing of Environment*, 64(1), 64–76.
- Wulder, M. A., White, J. C., Coops, N. C., & Butson, C. R. (2008). Multi-temporal analysis of high spatial resolution imagery for disturbance monitoring. *Remote Sensing of Environment*, 112(6), 2729–2740.
- Wunderle, A. L., Franklin, S. E., & Guo, X. G. (2007). Regenerating boreal forest structure estimation using SPOT-5 pan-sharpened imagery. *International Journal of Remote Sensing*, 28(19), 4351–4364.